Terminal settling velocity and physical properties of pollen grains in still air

Yuuki Hirose[1)*] and Kazuo Osada[1)#]

1: Graduate School of Environmental Studies, Nagoya University, Nagoya, Japan

* Presently at Panasonic Corporation, Osaka, Japan

#: Corresponding author

Corresponding author's e-mail address: kosada@nagoya-u.jp

Corresponding author's full postal address: Furo-cho, Chikusa-ku, Nagoya, 464-8601, Japan

Phone: +81-52-788-6049, Fax: +81-52-789-4306

Keywords: Pollen grain, Shape factors, Settling velocity, Aerodynamic diameter

Aerobiologia

September 2016, Volume 32, Issue 3, pp 385–394

DOI 10.1007/s10453-015-9408-0

Abstract

Numerical simulation of wind pollination requires knowledge of pollen grain physical parameters such as size, shape factor, bulk density, and terminal settling velocity. The pollen grain parameters for Japanese cedar, Japanese Cypress, short ragweed, Japanese black pine, and Japanese red pine were assessed for dry condition. Terminal settling velocities of dry pollen grains in still air were measured using image analysis of scattered light tracks in a dark settling tube. The measurement system was validated by comparing results to those obtained for standard microspheres of known size and density.

Dry pollen grain shape factors indicate closeness to sphere particles, except for pine pollen. Circularity factors of dry pine pollen grains were 0.90–0.86, suggesting more irregular shape than for other pollen species. Aerodynamic diameters of dry pollen grains were calculated based on the terminal settling velocity. Aerodynamic diameters of Japanese cedar, Japanese Cypress, and short ragweed closely resembled the projected area equivalent diameters, suggesting that aerodynamic behaviors of these pollen grains can be managed simply in numerical simulations. However, aerodynamic diameters of dry pine pollen grains were nearly 30% smaller than projected area equivalent diameters. Sacci on dry pine pollen can reduce the terminal settling velocity through low density and shape effects attributed to their non-sphericity, engendering aerodynamic diameter smaller by more than 10 μm from area equivalent diameters.

1 Introduction

Wind pollination is the major mode of pollen dispersion through the atmosphere, spreading pollen over a wide area. Recent studies have indicated that wind pollination engenders contamination between genetically modified and unmodified crops (Di-Giovanni and Kevan 1991; Watrud et al. 2004), and spreads allergens that cause rhinitis and other diseases to humans (Sofiev et al. 2013). Pollen from various plant species causes pollinosis (D'Amato et al. 2007; Lewis et al. 1983). In Japan, Japanese cedar (*Cryptomeria japonica*) and Japanese Cypress (*Chamaecyparis obtusa*) have been afforested extensively nationwide since the 1950s. As a result of increased cultivation of these young trees, pollinosis for cedar and Cypress has been increasing, becoming a severe national affliction in Japan (Okamoto et al. 2009; Yamada et al. 2014).

To predict the dispersion of pollen and to issue early warnings for pollinosis patients, many mesoscale numerical models have been developed (Efstathiou et al. 2011; Helbig et al. 2004; Kawashima and Takahashi 1995; Pasken and Pietrowicz 2005; Schueler and Schlünzen 2006; Sofiev et al. 2013; Zink et al. 2012). Among the various processes affecting pollen grain behavior in the atmosphere, the terminal settling velocity of pollen grains is an important parameter. For pollen grains, gravitational settling is the major mode of deposition, strongly controlling the suspension time in the atmosphere. The terminal settling velocity (V_{TS}) of a smooth spherical particle having diameter between about 1–70 μm can be estimated from Stokes's law as

$$V_{TS} = \frac{\rho_p d^2 g}{18\eta} \quad , \qquad (1)$$

where ρ_p stands for the particle density, d signifies the particle diameter, g denotes the gravitational constant, and η represents the fluid dynamic viscosity (Hinds 1999). As might be inferred from Eq. (1), for a given density, a larger particle will fall faster than a smaller one. Similarly, given particles of equal diameter, a heavier (denser) particle will fall faster than a lighter (looser) one. Consequently, data related to a pollen grain's diameter and density are crucial parameters to determine its time aloft in the atmosphere. Although the pollen grain diameter can be measured using optical and electron microscopy, the pollen grain density is difficult to ascertain (Gregory 1973). Hydration or desiccation of pollen grains also engenders difficulties for measuring the pollen grain diameter and density (Aylor 2002; Conner and Towill 1993; Griffith et al. 2012; Heslop-Harrison 1979; Katifori et al. 2010; van Hout and Katz 2004). In addition, the complex morphology of pollen grains might modify aerodynamic behavior during gravitational settling from the atmosphere because most pollen grains are non-spherical, with surface ornamentation including sacci or spines (Gregory 1973).

The terminal settling velocity of pollen grains has been measured using various experimental techniques. A simple and basic method has been to measure the time of settling for a certain distance in still air (e.g., Aylor 2002; Di-Giovanni et al. 1995; Ichikura and Iwanami 1981; Ukkelberg 1933; Zeleny and McKeehan 1910). Similarly, stroboscopic photography has been used to record the pollen grain settling speed (Niklas 1992; Schwendemann et al. 2007). A movie of particle settling was recorded using a video camera or computer-processed CCD camera and was used to analyze the terminal velocity (Loubet et al. 2007; Sawer

et al. 1994). Recently, high-speed digital inline holographic cinematography was used to measure the terminal velocity of ragweed, pine, and corn pollen (Sabban and van Hout 2011). Although these reports described terminal settling velocities for various pollen types, experimental data for important pollen causing pollinosis in Japan, especially for Japanese cedar, are scarce.

Aerodynamic behavior of saccate pollen, such as *Pinus strobus*, was studied mathematically (Schwendemann et al. 2007). Using a sophisticated numerical model, they investigated the settling velocity of pollen grains with and without sacci. Datasets including information related to terminal velocity, shape factor, and bulk density of pollen grains are necessary to ascertain the aerodynamic behavior of pollen grains in air. However, these datasets are rarely reported. Therefore, this study was conducted to obtain these datasets of dry pollen grains for Japanese cedar and other plants causing pollinosis and for Pines with sacci. Using these data, we will assess the relation between physical properties and aerodynamic diameters of pollen grains.

2 Materials and measurements

2.1 Materials

The terminal velocities of certified standard microspheres were measured before pollen grain measurements to assess data obtained from our experimental system. We used NIST traceable standard microspheres (catalog number 9000 series of Duke Standards) with nominal diameters of 10 μm (certified mean diameter: 9.9±1.0 μm, borosilicate glass), 20 μm (19.3±1.0 μm, soda lime glass), and 30 μm (30.1±1.1 μm, soda lime glass), all purchased from Thermo Fisher Scientific Particle Technology.

Pollen of Japanese cedar (*Cryptomeria japonica*), Japanese Cypress (*Chamaecyparis obtusa*), short ragweed (*Ambrosia artemisiifolia*), Japanese black pine (*Pinus thunbergii*), and Japanese red pine (*Pinus densiflora*) were purchased from the Japan Forest Tree Breeding Association and the Institute of Tokyo Environmental Allergy. These pollen samples were kept in a freezer at -18 °C to prevent degradation. Before conducting the experiments described below, about 0.1 g of pollen was placed on a petri dish and thawed at a room temperature. Although handling and drying methods are subject to investigation (Barajas et al., 2011; Conner and Towill, 1993), pollen was dried for 3 hr at 40 °C in a drying oven to ensure equal desiccation of pollen and stored in a desiccator with dried silica gel. Microscopic photographs of dried pollen grains were taken using digital microscope (VHX-5000; Keyence Corp.), as presented in Figs. 1 and 2.

2.2 Measurements

Size and shape factors

Particle size, height, and shape factors were ascertained using confocal laser scanning microscopy (CLSM, VK8700; Keyence Corp.) and image processing software (WinROOF; Mitani Corp.). Observation of size, height, and shape factors under CLSM was conducted on dried pollen grains immediately after brought from a desiccator. Pollen, such as *Pinus strobus* with sacci, might show preferential orientation during settling (Gregory 1973; Schwendemann et al. 2007). Therefore, to measure the pollen grain size and

shape factors for pine and Japanese cedar, we first investigated the preferential orientation during settling using a settling tube, as described later. For dried pine pollen, 46 out of 63 pollen grains landed with sacci pointing upward (Fig. 2). As Fig. 2 shows, the projection area of each dry pollen grain differs in grain orientation. For dried Japanese cedar pollen, 130 out of 149 pollen grains landed as papilla pointing upward. The result for pine pollen as sacci pointing upward agreed with results reported by Schwendemann et al. (2007). Consequently, the particle size and shape factors were measured for dry pollen grains as they stood with preferred orientation.

The projection area equivalent diameter (d_{PA}) is the diameter of a circle having the same projection area as the particle. It is estimated as

$$d_{PA} = 2\sqrt{\frac{A_p}{\pi}}\ , \qquad (2)$$

where A_p denotes the projected area measured using CLSM. For density estimation, which is described later, the projected area of dry pollen grain for pine and Japanese cedar was measured for all orientations, denoting the projection area equivalent diameter for all orientation (d_{AO}).

The circularity factor (*CF*), an indicator of closeness to perfect circle, is estimated as

$$CF = \frac{4\pi A_p}{L^2}\ , \qquad (3)$$

where *L* stands for the periphery length based on image analysis. For a perfect circle, *CF* equals 1.

The aspect ratio (*AR*) is defined as a proportional relation between the longest dimension and orthogonal width of the particle. It is estimated as

$$AR = \frac{a}{b}, \qquad (4)$$

where *a* stands for longest dimension and *b* denotes the orthogonal width based on image analysis.

We also define the pole to equator ratio (*PER*) as a ratio between the height (*h*) of a particle measured by CLSM and the d_{PA} of the particle. It is estimated as shown below.

$$PER = \frac{h}{d_{PA}} \qquad (5).$$

The particle size of standard microspheres was measured to assess the accuracy of image analysis using CLSM and WinROOF. The measured projection area equivalent diameters (30.3±1.6 μm, 20.1±1.4 μm, and 10.5±0.8 μm) showed reasonable agreement with the certified value (30.1±1.1 μm, 19.3±1.0 μm, and 9.9±1.0 μm, respectively). The median values of *CF* and *AR* for the standard microspheres were 0.95–0.98 and 1.03–1.07, respectively, showing slight deviation from perfect spheres. Deviations from perfect circles imply error margins for our measurements.

Terminal settling velocity

The terminal settling velocity was estimated from the length of the scattered light track per unit time for dry pollen grain settling. Figure 3 presents a schematic diagram of the experimental layout including a transparent settling tube (4.5 cm inner diameter, 1.2 m length made by polycarbonate sprayed inside with antistatic coatings), a laser light source (a semiconductor laser pointer emitting wavelength 635 nm, 1 mW), a video camera recorder (GZ-HM670; JVC–Kenwood Holdings Corp.), and a sieve. Measurements were

taken in a dark room. A transparent plastic cover was fitted at the bottom of the tube to inhibit convection flow inside the tube. Vertical air movements by thermal and turbulent convection in the tube might bias experimentally obtained results. Similarly to Aylor (2002), we confirmed the absence of air movement in the tube by introducing a smoke tracer (aerosol particles of propylene glycol having diameter about 1–10 μm) produced by an airflow indicator (AF-1; Komyo Rikagaku Kogyo K.K.). Results show that smoke remained stationary without movement for a sufficiently long time unless the plastic cover had been removed.

A sieve at the tube top was used to introduce a single particle or pollen grain selectively. The mesh sizes were 53 μm, 25 μm, and 15 μm depending on the target particle size. The laser beam illuminated the settling particles from below. Light scattered by settling particles was recorded using a video camera placed at about 40 cm below the sieve, where particles reached terminal settling velocities. The video camera shutter speed was 30 segments per second according to the product specifications. By playing back the video record frame-by-frame, the terminal settling velocity of the particles can be estimated from the light track length. Using digital imaging software (Image J; Schneider et al., 2012), 10 consecutive still images were used to measure the length of each light track per unit time. Consequently, the terminal settling velocity of a particle or grain was calculated as an average of measurements for 10 consecutive light tracks of a particle.

Our measurement system for the terminal settling velocity was verified using certified standard microspheres. Measured average settling velocities for 30 μm, 20 μm, and 10 μm were, respectively, 6.5±0.3 cm s^{-1}, 2.7±0.2 cm s^{-1}, and 0.9±0.1 cm s^{-1}. We also calculated the terminal settling velocity for the standard microspheres by introducing their certified diameters and densities with dynamic viscosity of air ($\eta=17.5\times10^{-6}$ Pa s) to Stokes's law (Eq. 1). Measured values agreed well with predicted terminal settling velocities of 6.9±0.1 cm s^{-1}, 2.9±0.1 cm s^{-1}, and 0.8±0.0 cm s^{-1}, respectively, for 30 μm, 20 μm, and 10 μm.

Bulk density of pollen grains

The bulk density of dried pollen grains was obtained by weighing and counting dry pollen grains as filter residues. Pollen grains were dispersed in water and were filtered through Nuclepore filters (1 μm pore size; Whatman Co. Ltd.). The concentrations and amounts of aliquots were adjusted to form a single layer of hydrated pollen grains as a residue on the filter. The filter was dried at 40 °C for 5 hr and was weighed up to 0.01 mg using an electronic microbalance (GH-252; A&D Co. Ltd.). Microscopic photographs of dry pollen grains on the filter were taken using CLSM at 400× for Japanese cedar, Japanese Cypress, and short ragweed, and 200× for Japanese black and red pines to cover all areas of the filter residue. The dry pollen grains were counted using the WinROOF software and were summed up as the total number on the filter. Assuming the dried pollen grain as a spherical particle, bulk density (ρ) was calculated as shown below.

$$\rho=\frac{6}{\pi d^3}\cdot\frac{\mathrm{m}}{\mathrm{n}} \quad (6)$$

Therein, d stands for the mean diameter, m represents the weight of the residue, and n denotes the total number of dry pollen grains counted on the filter. We used d_{PA} as d for Japanese Cypress and short ragweed, and d_{AO} as d for pine and Japanese cedar. Grain volume measured by CLSM is usually overestimated for space underneath of grain. Therefore, we use d_{AO} or d_{PA} instead of volume data measured by CLSM.

Aerodynamic diameter

The aerodynamic diameter (d_a), a parameter characterizing the aerodynamic behavior of a particle, is defined for a particle as the diameter of the spherical particle with density of 1 g cm^{-3} having the same terminal settling velocity as the particle (Hinds, 1999). The aerodynamic diameter can be expressed as

$$d_a = \sqrt{\frac{18\eta V_{TS}}{\rho_0 g}}, \quad (7)$$

where V_{TS} stands for the measured terminal velocity, ρ_0 signifies the standard density (1 g cm^{-3}) as defined, and g is the gravitational constant.

3 Results and discussion

Table 1 presents results of pollen grain measurements. The projection area equivalent diameter (d_{PA}) of dry pollen grains ranged from 21 (ragweed) to 46 (Japanese black pine) μm. Although the absolute value of standard deviations of d_{PA} was smaller for ragweed (1.3 μm) than for Japanese red pine (2.6 μm), the largest and the smallest relative standard deviations to d_{PA} were obtained for Japanese cedar and Japanese black pine (7.0% and 4.8%, respectively). Regarding the circularity factor (*CF*), lower values (0.86 and 0.90) were obtained respectively for dry pollen grains of Japanese red and black pine. *CF* values for the other three species were around 0.95. The standard deviations (0.02) of *CF* for Japanese cedar, Japanese Cypress, and short ragweed were much smaller than those for pine grains (0.10–0.16). Lower *CF* values with larger standard deviations of *CF* for pine species are consistent with a larger standard deviation of d_{PA} and are attributed to the existence of sacci, as presented in Fig. 1 and Fig. 2. Sacci makes complex morphology of pollen grains, so that the grain shape tends to deviate from a smooth circle or sphere. The aspect ratio (*AR*) of dry pollen grains ranged from 1.06 (Japanese cedar and Short ragweed) to 1.17 (Japanese Cypress), all showing values nearly equal to 1.1. The pole-to-equator ratio (*PER*) for dry pollen grains was around 0.95, with a minimum of 0.91 (Japanese cedar) and a maximum of 1.03 (Short ragweed). Based on these parameters, although the surface texture of pollen grains is not smooth, the shape of dry pollen grains measured in this study can be approximated as a spherical particle.

Fig. 4 presents frequency distributions of the measured terminal settling velocities (V_{TS}) of dry pollen grains. The average V_{TS} for dry pollen grains of the five species is also presented in Table 1. The average V_{TS} were 1.03 (short ragweed) to 3.2 (Japanese black pine) cm s^{-1}. Faster V_{TS} was obtained for larger grains, which is fundamentally consistent with Stokes's law. The relative standard deviations of V_{TS} were less than 10%, except for short ragweed. As portrayed in Fig. 4c, V_{TS} for short ragweed was 0.7–1.7, exhibiting extremely large variation. The relative standard deviation of d_{PA} for short ragweed was only 6%. Therefore, the large variation of V_{TS} might be attributed to reasons other than the size variation of dry grains. One reason might be the measurement difficulty of light track detection for short ragweed because of small grains.

Many reports have described V_{TS} of various pollen grains, but reliable V_{TS} with grain size data are rare, especially for species in this study. Validation of measurement systems for V_{TS} can be made by application

of reference particles, as reported by Zeleny and McKeehan (1910), Sawyer et al. (1994), Loubet et al. (2007), and Sabban and van Hout (2011). Among those reports, only that of Sabban and van Hout (2011) provided V_{TS} with d_{PA} for short ragweed (*Ambrosia artemisiifolia*) and pine (*Pinus Taeda*). As presented in Table 2, their V_{TS} (1.36±0.18 cm s^{-1}) for ragweed (21±1 μm) agrees well with our value (1.2±0.2 cm s^{-1}, d_{PA}=21.3±1.3 μm). For pine (d_{PA}= 51±4 μm), V_{TS} was 4.04±0.73 cm s^{-1}, which is slightly higher than our values, probably because of differences of species and grain size. Without validation of the measurement system, Durham (1946) reported V_{TS} for short ragweed and pine. Furthermore, lacking validation of measurements, Ichikura and Iwanami (1981) reported V_{TS} for various pollen species obtained in Japan. These data differ from our values, although the V_{TS} of Japanese black pine closely approximates our data.

Schwendemann et al. (2007) developed a numerical model to ascertain the effects of sacci of pine. They numerically estimated that V_{TS} of pine (*Pinus strobus*, d_{PA}= 51 μm) was 3.07±0.31 cm s^{-1}. Considering the pine pollen size, their estimated V_{TS} was slightly slower than our value.

Table 1 shows bulk densities of dry pollen grains using d_{PA} for Japanese Cypress and short ragweed, and d_{AO} for Japanese black pine, Japanese red pine and Japanese cedar. The values of d_{PA} are always larger than d_{AO} because of larger resistance for preferred settling orientation. Based on a similar method (Durham 1943) used for this study, Durham (1946) reported the density of short ragweed (*Ambrosia elatior*) as 0.55 g cm^{-3}. Harrington and Metzger (1963) found the density (0.84 g cm^{-3}) of short ragweed (*Ambrosia artemisiifolia*) using a Beckman gas pycnometer. The density (0.71±0.09 g cm^{-3}) of short ragweed found in this study is in the middle of previously reported values. Two examples of numerical model simulations for ragweed dispersion are also presented in Table 2. V_{TS} used in Efstathiou et al. (2011) was similar to our value but they used much higher density than ours. In contrast, Zink et al. (2012) applied density similar to this study. For pine pollen, Durham (1946) reported density of 0.45 g cm^{-3} both for *Pinus sylvestris* and *Pinus ponderosa*. Although the pine species differ, the lower (ca 0.5 g cm^{-3}) density agrees with our measurements.

Density of pollen grain is not easy to ascertain because of uncertainty derived from hydration/desiccation, various void on the grain surface, and difficulty of measuring average diameter of grains. Assuming aerodynamic shape factor equals unity, another way to estimate density is to solve Stokes's equation (equation 1) by application of measured d and V_{TS}. As an example of dry grain that has nearly spherical shape, density of short ragweed is calculated as 0.85 g cm^{-3}. The estimated density is close to measured density of Harrington and Metzger (1963) and 16% higher than measured value in this study. Similarly, density is calculated as 0.97 g cm^{-3} for Japanese Cypress, which is 15% higher than measured value in this study.

Table 1 presents aerodynamic diameters (d_a) calculated from V_{TS} in this study. Comparing d_a with d_{PA} in Table 1, d_a of Japanese cedar, Japanese Cypress, and short ragweed were nearly equal to d_{PA} (relative differences are less than 8%). This fact is extremely important for simulating the atmospheric behavior of these dry pollen grains. Actually, d_a for these dry pollen grains can be approximated as d_{PA} in numerical simulations. As pointed out by Tang et al. (2004), higher particle surface roughness increases the particle drag force as it settles. Therefore, it reduces V_{TS} and d_a. Although the pollen grain surface roughness was

not measured in this study, the values of measured shape factors were approximately spherical, as discussed earlier. Therefore, d_a is close to d_{PA} for Japanese cedar, Japanese Cypress, and short ragweed.

However, the differences between d_a and d_{PA} for Japanese black pine and Japanese red pine were greater than 10 μm. The relative differences were approximately 30%, suggesting that aerodynamic behavior (values for d_{PA} and ρ or V_{TS}) must be considered for proper simulation of pine pollen in the atmosphere. Schwendemann et al. (2007) reported that V_{TS} (3.07±0.31 cm s^{-1}) for *Pinus strobus* grains with sacci was slower than V_{TS} (3.40±0.37 cm s^{-1}) for the same species without sacci. Adding a light weight but large volume of sacci to a pollen grain can reduce V_{TS} because of increased drag force as the whole grain. In fact, the bulk density of dry pollen grains for pine was low (0.55 g cm^{-3}). In addition, *CF* values (0.90 and 0.86 for Japanese black pine and red pine, respectively) were lower than those for other species. These low values might be a reason for the increased drag force of pollen grains during settling.

5 Summary and conclusions

Grain size, shape factors, terminal settling velocity, and bulk density of dry pollen grains were obtained for Japanese cedar, Japanese Cypress, short ragweed, Japanese black pine, and Japanese red pine. Grain size and shape were analyzed using confocal laser scanning microscopy and image processing software. Terminal settling velocities of dry pollen grains in still air were estimated from image analyses of scattered light tracks in a dark settling tube. The measurement system was validated through comparison to standard microspheres.

Aside from pine pollen, values of dry pollen grain shape factors showed that they were approximately spherical particles. For dry pine pollen grains, circularity factors and bulk densities were 0.90–0.86 and about 0.55 g cm^{-3}, respectively, suggesting an irregular shape of projection images and lower bulk densities than those of other pollen species. Based on the measured settling velocity, aerodynamic diameters of dry pollen grains were also calculated. Aerodynamic diameters of Japanese cedar, Japanese Cypress, and short ragweed were close to projection area equivalent diameters. However, the aerodynamic diameters of Japanese black pine, and Japanese red pine were more than 10 μm smaller than the projection area equivalent diameters. Existence of sacci on dry pine pollen grains reduces V_{TS} through lowering of the bulk density and increasing of the shape irregularity of dry pollen grains.

Acknowledgements

This research was supported financially by JSPS KAKENHI Grant Nos. 23310004, 25220101, and 15H02803, and by the Environment Research and Technology Development Fund (5B-1202) of the Ministry of the Environment, Japan. We thank Keyence Corp. for the use of the newest digital microscope VHX-5000.

References

Aylor, D. E. (2002). Settling speed of corn (*Zea mays*) pollen. Journal of Aerosol Science, 33, 1601–1607.

Barajas, J., Cortes-Rodriguez, M., and Rodriguez-Sandoval, E. (2012). Effect of temperature on the drying

process of bee pollen from two zones of Colombia. Journal of Food Process Engineering, 35(1), 134–148.

Connor, K. F., & Towill, L. E. (1993). Pollen-handling protocol and hydration/dehydration characteristics of pollen for application to long-term storage. Euphytica, 68(1-2), 77–84.

D'Amato, G., Cecchi, L., Bonini, Z., Nunes, C., Annesi-Maesano, I., Behrendt, H. et al. (2007). Allergenic pollen and pollen allergy in Europe. Allergy, 62, 976–990.

Di-Giovanni, F., & Kevan, E G. (1991). Factors affecting pollen dynamics and its importance to pollen contamination: a review. Canadian Journal of Forest Research, 21, 1155–1170.

Di-Giovanni, F., Kevan, P. G., & Nasr, M. E. (1995). The variability in settling velocities of some pollen and spores. Grana, 34, 39–44.

Durham, O. C. (1943). The volumetric incidence of atmospheric allergens: I. Specific gravity of pollen grains. Journal of Allergy, 14(6), 455–461.

Durham, O. C. (1946). The volumetric incidence of atmospheric allergens. III. Rate of fall of pollen grains in still air. Journal of Allergy, 17, 70–78.

Efstathiou, C., Isukapalli, S., & Georgopoulos, P. (2011). A mechanistic modeling system for estimating large-scale emissions and transport of pollen and co-allergens. Atmospheric Environment, 45(13), 2260–2276.

Gregory, P. H. (1973). *The microbiology of the atmosphere*. Second ed. John Wiley & Sons, New York, Toronto.

Griffiths, P. T., Borlace, J. S., Gallimore, P. J., Kalberer, M., Herzog, M., & Pope, F. D. (2012). Hygroscopic growth and cloud activation of pollen: a laboratory and modelling study. Atmospheric Science Letters, 13(4), 289–295.

Harrington, J. B., Jr., & Metzger, K. (1963). Ragweed pollen density. American Journal of Botany, 50, 532–539.

Helbig, N., Vogel, B., Vogel, H., & Fiedler, F. (2004). Numerical modelling of pollen dispersion on the regional scale. Aerobiologia, 20(1), 3–19.

Heslop-Harrison, J. (1979). Pollen Walls as Adaptive Systems. Annals of the Missouri Botanical Garden, 66, 813–829

Hinds, W. C. (1999). *Aerosol technology: Properties, behavior, and measurement of airborne particles.* Wiley, New York.

Ichikura, M., & Iwanami, Y. (1981). Studies of fall-velocity of pollen grains. Japanese Journal of Palynology, 27, 5–13.

Katifori, E., Alben, S., Cerda, E., Nelson, D. R., & Dumais, J. (2010). Foldable structures and the natural design of pollen grains. Proceedings of the National Academy of Sciences, 107(17), 7635–7639.

Kawashima, S., & Takahashi, Y. (1995). Modelling and simulation of mesoscale dispersion processes for airborne cedar pollen. Grana, 34, 142–150

Lewis, W. H., Vinay, P., & Zenger, V. E. (1983). *Airborne and allergenic pollen of North America*. Johns Hopkins University Press.

Loubet, B., Jarosz, N. Saint-Jean, S., & Huber, L. (2007). A method for measuring the settling velocity distribution of large biotic particles. Aerobiologia, 23, 159–169.

Niklas, K. J. (1992). *Plant biomechanics: an engineering approach to plant form and function*. University of Chicago Press, Chicago, Illinois, USA.

Okamoto, Y., Horiguchi, S., Yamamoto, H., Yonekura, S., & Hanazawa, T. (2009). Present Situation of Cedar Pollinosis in Japan and its Immune Responses. Allergology International, 58, 155–162.

Pasken, R., & Pietrowicz, J. A. (2005). Using dispersion and mesoscale meteorological models to forecast pollen concentrations. Atmospheric Environment, 39(40), 7689–7701.

Sabban, L., & van Hout, R. (2011). Measurements of pollen grain dispersal in still air and stationary, near homogeneous, isotropic turbulence. Journal of Aerosol Science, 42, 867–882.

Sawyer, A. J, Griggs, M. H., & Wayne, R. (1994). Dimensions, density, and settling velocity of Entomophthoralean Conidia: Implications for aerial dissemination of Spores. Journal of Invertebrate Pathology, 63, 43–55.

Schneider, C. A., Rasband, W. S., & Eliceiri, K. W. (2012). NIH Image to Image J: 25 years of image analysis. Nature Methods, 9, 671–675.

Schueler, S., & Schlünzen, K. H. (2006). Modeling of oak pollen dispersal on the landscape level with a mesoscale atmospheric model. Environmental Modeling & Assessment, 11(3), 179–194.

Schwendemann, A. B., Wang, G., Mertz, M. L., McWilliams, R. T., Thatcher, S. L., & Osborn, J. M. (2007). Aerodynamics of saccate pollen and its implications for wind pollination, American Journal of Botany, 94, 1371–1381.

Sofiev, M., Belmonte, J., Gehrig, R., Izquierdo, R., Smith, M., Dahl, Å. et al. (2013). Airborne pollen transport, In M. Sofiev and K-C. Bergmann (Eds), *Allergenic Pollen: A Review of the Production, Release, Distribution and Health Impacts,* Springer Science+Business Media, Dordrecht.

Tang, P., Chan, H.-K., & Raper, J. A. (2004). Prediction of aerodynamic diameter of particles with rough surfaces. Powder Technology, 147, 64–78.

Ukkelberg, H. G. (1933). The rate of fall of spores in relation to the epidemiology of black stem rust. Bulletin of the Torrey Botanical Club, 60, 211–228

van Hout R., & Katz, J. (2004). A method for measuring the density of irregularly shaped biological aerosols such as pollen. Journal of Aerosol Science, 35, 1369–1384.

Watrud, L. S., Lee, E. H., Fairbrother, A., Burdick, C., Reichman, J. R., Bollman, M. et al. (2004). Evidence for landscape-level, pollen-mediated gene flow from genetically modified creeping bentgrass with CP4 EPSPS as a marker. Proceedings of the National Academy of Sciences of the United States of America, 101, 14533–14538.

Yamada, T., Saito, H., & Fujieda, S. (2014). Present state of Japanese cedar pollinosis: The national affliction. Journal of Allergy and Clinical Immunology, 133, 632–639.

Zeleny, J., & McKeehan, L. W. (1910). The terminal velocity of fall of small spheres in air. Phys. Rev. (Series I), 30, 535–560.

Zink, K., Vogel, H., Vogel, B., Magyar, D., & Kottmeier, C. (2012). Modeling the dispersion of *Ambrosia*

artemisiifolia L. pollen with the model system COSMO-ART. International Journal of Biometeorology, 56(4), 669–680.

Figure captions

Fig. 1 Photographs of dried pollen grains taken at ×2000 magnification: (a) Japanese cedar, (b) Japanese Cypress, (c) short ragweed, (d) Japanese black, pine, and (e) Japanese red pine. Red bar shows 10 μm scale.

Fig. 2: Photograph of dried pollen grains for Japanese red pine taken at ×500 magnification. Dry pollen grains are randomly oriented in this photograph. Red bar shows 100 μm scale.

Fig. 3: Schematic diagram of measurement system used for this study.

Fig. 4: Frequency distribution of the terminal settling velocity for various dry pollen grains: (a) Japanese cedar, (b) Japanese Cypress, (c) short ragweed, (d) Japanese black pine, and (e) Japanese red pine.

Table 1. Summary of projection area equivalent diameter for settling direction (d_{PA}), circularity factor (*CF*), aspect ratio (*AR*), pole to equator ratio (*PER*), terminal settling velocity (V_{TS}), projection area equivalent diameter for all direction (d_{AO}), bulk density (ρ), and aerodynamic diameter (d_a) of dry pollen grains

# of samples	d_{PA} (μm)	*CF*	*AR*	*PER*	V_{TS} (cm s-1)	d_{AO}	ρ (g cm-3)	d_a (μm)
Japanese cedar								
36	28.4±2.0	0.95±0.02	1.06±0.04	0.91±0.08	–		–	–
81	–	–	–	–	2.3±0.2		–	27.2±0.4
88	–	–	–	–	–	27.0±2.6	–	–
3	–	–	–	–	–		1.06±0.08	–
Japanese Cypress								
66	27.6±1.9	0.94±0.02	1.17±0.11	0.96±0.09	–	–	–	–
44	–	–	–	–	2.3±0.2	–	–	27.2±0.4
3	–	–	–	–	–	–	0.82±0.04	–
Short ragweed								
41	21.3±1.3	0.95±0.02	1.06±0.04	1.04±0.08	–	–	–	–
20	–	–	–	–	1.2±0.2	–	–	19.6±0.4
2	–	–	–	–	–	–	0.71±0.09	–
Japanese black pine								
38	45.7±2.2	0.90±0.10	1.12±0.07	0.94±0.03	–	–	–	–
68	–	–	–	–	3.2±0.3	–	–	32.1±0.5
84	–	–	–	–	–	41.7±3.7	–	–
3	–	–	–	–	–	–	0.55±0.03	–

Japanese red pine								
36	43.9±2.6	0.86±0.16	1.13±0.08	0.95±0.04	–	–	–	–
55	–	–	–	–	3.1±0.2	–	–	31.6±0.5
94	–	–	–	–	–	40.9±3.2	–	–
3	–	–	–	–	–	–	0.54±0.04	–

Table 2. Comparison of data from other studies

Species	d_{PA} (μm)	V_{TS} (cm s^{-1})	ρ (g cm^{-3})	ref
Short ragweed	21.3±1.3	1.2±0.2	0.71±0.09	this study
Ambrosia artemisiifolia	21±1	1.36±0.18		1
# *Ambrosia elatior*	20.0	0.88	0.55	2
# *Ambrosia artemisiifolia*	19	2.5		3
Ambrosia artemisiifolia	-	-	0.84	4
input parameter	20	1.1	1.20	5
input parameter	20	-	0.83	6
Pine				
#*Pinus sylvestris*	52.0	2.5	0.45	2
#*Pinus ponderosa*	60.0	3.5	0.45	2
# *Pinus strobus*	51	3.07±0.31		7
Japanese black pine	45.7±2.2	3.2±0.3	0.55±0.03	this study
#*Pinus thunbergii*	48.5	3.6		3
Japanese red pine	43.9±2.6	3.1±0.2	0.54±0.04	this study
Pinus taeda	51±4	4.04±0.73		1
Japanese Cypress	27.6±1.9	2.3±0.2	0.82±0.04	this study
#*Chamaecyparis obtusa*	34	3.2		3

# indicates measurements without validation for V_{TS}.

References: 1, Sabban and Hout (2011); 2, Durham (1946); 3, Ichikura and Iwanami (1981); 4, Harrington and Metzger (1963); 5, Efstathiou et al. (2011); 6, Zink et al. (2012); 7, Schwendemann et al. (2007).

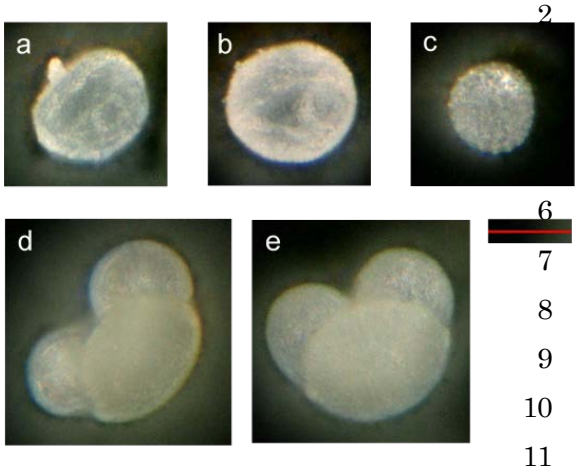

Fig. 1 Photographs of dried pollen grains taken at ×2000 magnification: (a) Japanese cedar, (b) Japanese Cypress, (c) short ragweed, (d) Japanese black pine, and (e) Japanese red pine. Red bar shows 20 μm scale.

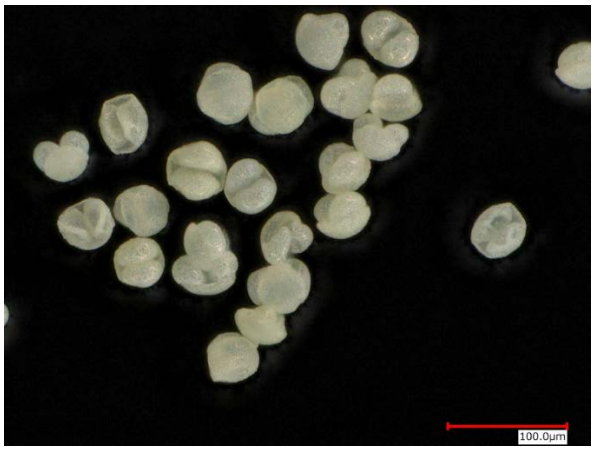

Fig. 2: Photograph of dried pollen grains for Japanese red pine taken at ×500 magnification. Pollen grains are randomly oriented in this photograph. Red bar shows 100 µm scale.

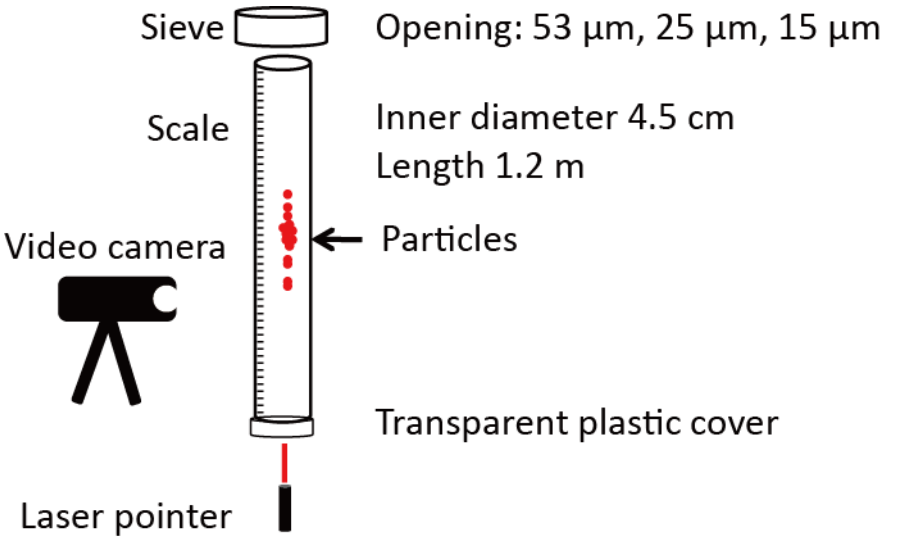

Fig. 3: Schematic diagram of measurement system used for this study.

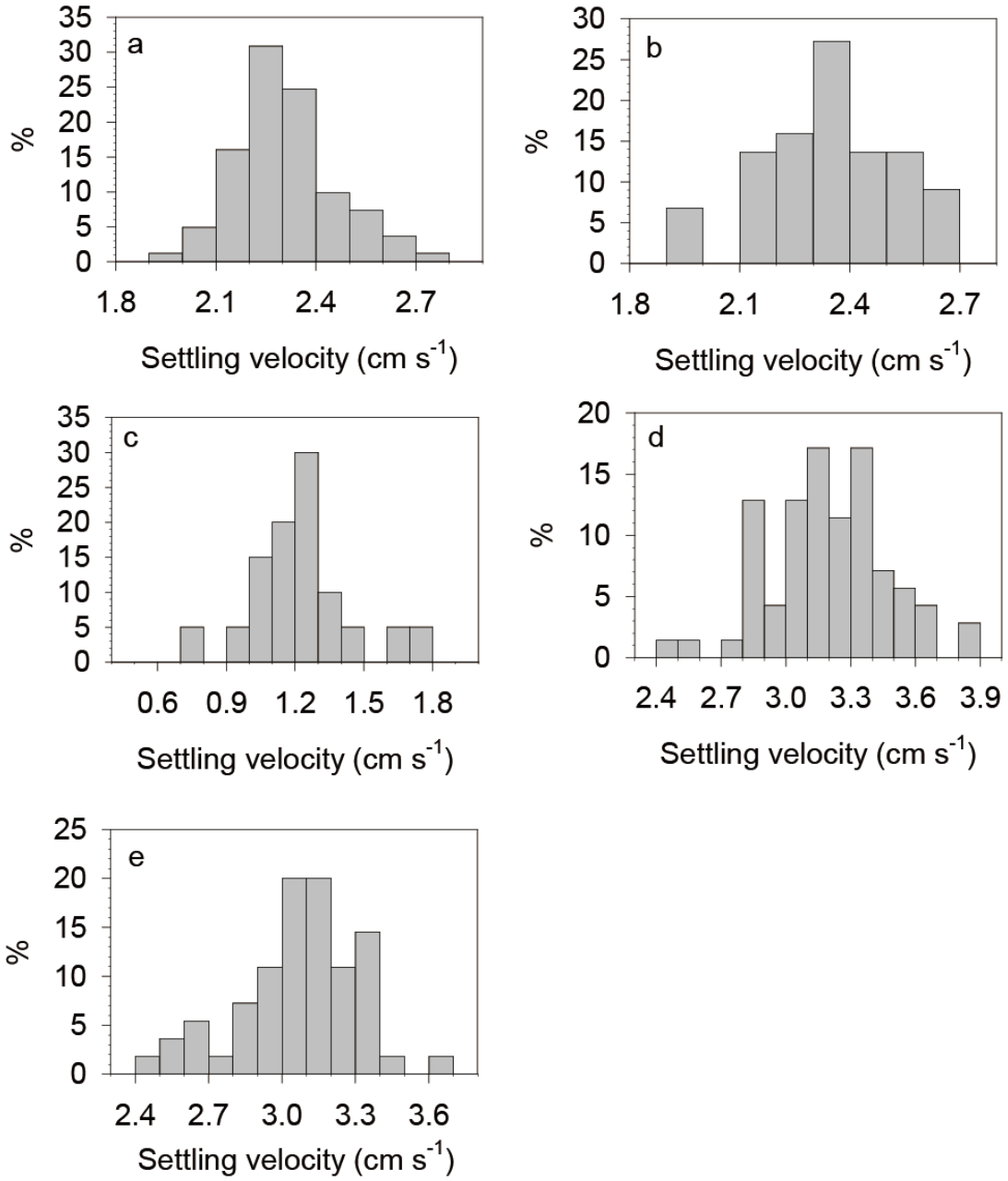

Fig. 4: Frequency distribution of the terminal settling velocity for various dry pollen grains: (a) Japanese cedar, (b) Japanese Cypress, (c) short ragweed, (d) Japanese black pine, and (e) Japanese red pine.